From the Hénon conservative map to the Chirikov standard map for large parameter values

Narcís Miguel, Carles Simó and Arturo Vieiro

Dept. de Matemàtica Aplicada i Anàlisi, Universitat de Barcelona, Gran Via 585, 08007, Barcelona, Catalunya

narcis@maia.ub.es carles@maia.ub.es vieiro@maia.ub.es

Abstract

In this paper we consider conservative quadratic Hénon maps and Chirikov's standard map, and relate them in some sense.

First, we present a study of some dynamical properties of orientation-preserving and orientation-reversing quadratic Hénon maps concerning the stability region, the size of the chaotic zones, its evolution with respect to parameters and the splitting of the separatrices of fixed and periodic points plus its role in the preceding aspects.

Then the phase space of the standard map, for large values of the parameter, k, is studied. There are some stable orbits which appear periodically in k and are scaled somehow. Using this scaling, we show that the dynamics around these stable orbits is the one of above Hénon maps plus some small error, which tends to vanish as $k \to \infty$. Elementary considerations about diffusion properties of the standard map are also presented.

Dedicated to our friend Sergey Gonchenko on his 60th birthday

1 Introduction

The universal character of the Hénon map (1) is well-known since, in particular, it appears as a return map close to a quadratic tangency in the dissipative setting [1, 2]. Later the conservative orientation-preserving Hénon map (1) was obtained as a universal return map for quadratic tangencies of conservative maps preserving orientation, see, for instance, [3, 4, 5]. Recently, it has been proved that the orientation-reversing Hénon map also appears as a universal return map in non-orientable cases, either for maps defined in non-orientable manifolds or for hyperbolic points with eigenvalues λ and μ such that $\lambda\mu = -1$, see [6]. On the other hand, in [7] the authors consider non-transversal heteroclinic cycles for reversible maps having symmetric saddle fixed points, and they show that the corresponding return map can be written as the composition of either two orientation-preserving or two orientation-reversing Hénon maps.

In this work we investigate both orientation-preserving and orientation-reversing cases. Several properties concerning the stability region, the size of the chaotic zones, the splitting of separatrices of the fixed/periodic points, etc, are presented in Sections 2 and 3.

In Section 4 we perform an extensive numerical exploration of the relative regular area of the phase space of Chirikov's standard map [8] for large values of the parameter, by means of the computation of Lyapunov exponents. This allows us to detect stable islands appearing periodically in the parameter that show some scaling properties.

In Section 5 we analyse the properties of such little islands, which are of period 1, 2 and 4. More concretely, we focus on the renormalisation properties of these islets and we derive suitable limit maps. It turns out that the obtained limit maps correspond to the orientation-preserving Hénon map, the composition of two of these and the composition of two orientation-reversing Hénon maps, respectively. The results obtained fit within the same spirit of previous results in [8, 9]. The effect of these islets of stability in the diffusion properties of the Chirikov standard map are also analysed by means of the elementary quasi-linear approximation of the diffusion coefficient.

2 The Hénon conservative orientation-preserving map

In 1969 M. Hénon [10] started the study of quadratic area preserving maps in $\mathbb{R}^2$. He proved that quadratic maps with constant Jacobian can be reduced to the form

$$F:(x,y)\to(1-ax^2+y,bx) \tag{1}$$

for some constants $a,b\in\mathbb{R}$, with minors exceptions. If $b=-1$ the map is area and orientation-preserving. If $b=1$ it is area preserving and orientation-reversing. The case $b=-1$ has a very simple geometric interpretation as the composition of two maps. The first one is $(x,y)\to(x,y+1-ax^2)$, one of the so-called "de Jonquières" maps, while the second is just a rotation by an angle of $-\pi/2$.

However, in what follows, we use another representation of the case $b=-1$ given by:

$$HP_c:\begin{pmatrix} x\\ y\end{pmatrix}\to\begin{pmatrix} x+2y+\frac{c}{2}(1-(x+y)^2)\\ y+\frac{c}{2}(1-(x+y)^2)\end{pmatrix}, \tag{2}$$

where it is enough to consider $c>0$. We name it HP which stands for Hénon orientation-preserving map. This representation is obtained from a minimal modification of the version given in [11]: $F_c:(x,y)\to(c(1-x^2)+2x+y,-x)$ after the change $(X,Y)=(x-y,x+y)/2$, and renaming (X,Y) as (x,y). The subscript c in these maps is introduced to stress that they depend on this parameter. The map (2) has two fixed points. One of them, H, is located at $(-1,0)$ and it is hyperbolic for all $c>0$. The other one, E, located at $(1,0)$, is elliptic for $0<c<2$, parabolic for $c=2$ and reflection hyperbolic for $c>2$.

2.1 Symmetries, reversors, limit flow and rotation number

The inverse map can be expressed as $HP_c^{-1}=S\circ HP_c\circ S$, where S is the symmetry given by $S(x,y)=(x,-y)$. Defining $R=S\circ HP_c$, which is clearly an involution like S, we have $HP_c=S\circ R$ and $HP_c^{-1}=R\circ S$. Both S and R are called reversors. We can consider the sets, $\mathrm{Fix}(S)$ and $\mathrm{Fix}(R)$, of fixed points of both reversors, i.e., either points $z=(x,y)$ such that $S(z)=z$ (which are the points with $y=0$) or points such that $R(z)=z$, which belong to a parabola.

A reversor like S plays an important role to locate periodic points on $\mathrm{Fix}(S)$. If for a point $p\in\mathrm{Fix}(S)$ there exists $m\in\mathbb{N}$ such that $HP_c^m(p)\in\mathrm{Fix}(S)$, then p is periodic, of period m if $p=HP_c^m(p)$ and of period $2m$ if $p\neq HP_c^m(p)$. Furthermore, for any of these periodic points, if it is hyperbolic, the image under S of the unstable manifold $W^u(p)$ is the stable one $W^s(p)$. Similar properties hold for the reversor R.

For a preliminary study of the dynamics of an arbitrary map F, provided it is close to the identity map, Id, it is quite useful to look for the existence of some ODE such that the time-1 map associated with the flow gives a good approximation to F. In the case of

(2) this can be done by introducing the new variables $(\xi,\eta)=(x,2y/\sqrt{c})$. Then, in the (ξ,η) variables, HP_c differs from Id by $\mathcal{O}(\sqrt{c})$. A scaling of time also by $\sqrt{c}$ leads to:

$$\frac{d\xi}{dt}=\eta, \quad \frac{d\eta}{dt}=1-\xi^2, \tag{3}$$

an ODE which is Hamiltonian with $H(\xi,\eta)=\frac{1}{2}\eta^2-\xi+\frac{1}{3}\xi^3$. The solutions are contained in the level curves of H and the main features are shown in the elementary Figure 1 left. It has also $H=(-1,0)$ and $E=(1,0)$ as fixed points, of hyperbolic and elliptic type respectively. The level $H^{-1}(2/3)$ contains the separatrix. Points inside the domain bounded by the separatrix belong to a foliation of periodic solutions. In the right side plot we show some confined orbits for HP_c, as well as the right branches of the invariant manifolds of the hyperbolic fixed point. They seem to be coincident but, of course, they are not (see Section 2.4). For this small value of c the main difference between both plots is the change in the y variable by a factor $\sqrt{c}/2$ when going from the left plot to the right one.

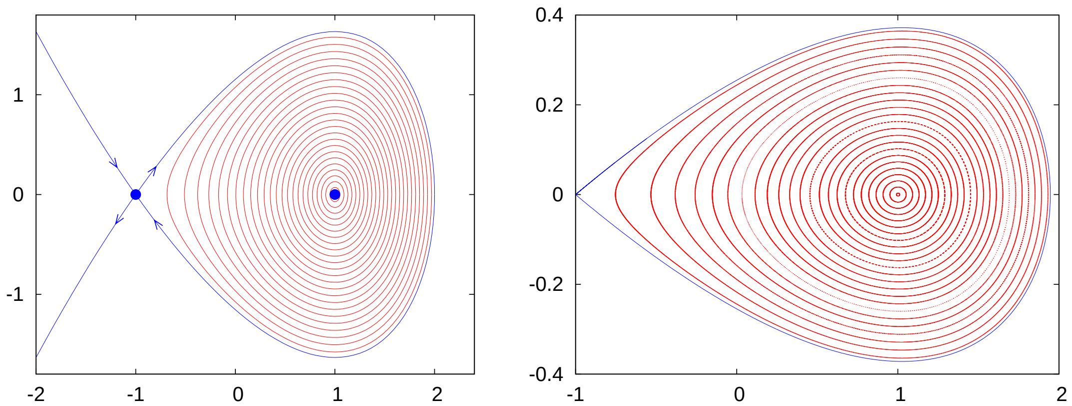

Figure 1: Left: the phase portrait of system (3). Fixed points are shown in blue, as are the invariant manifolds of the hyperbolic point. The periodic orbits are shown in red. Right: the right branches of the invariant manifolds of the hyperbolic point and (part of) the orbits of several initial points under HP_c, for $c=0.2$.

An extremely relevant parameter is the rotation number. If we consider the time-$\sqrt{c}$ map associated to the flow, the rotation number corresponding to a periodic orbit of period T is $\rho=\sqrt{c}/T$. It decreases monotonically from $\sqrt{c}/(\sqrt{2}\pi)$ to 0 when going from E to H. The values agree very well with the corresponding rotation numbers for HP_c, for c small, when ρ is defined, i.e., on the curves invariant under HP_c.

For increasing values of c the rotation number, when it is defined, gives a very good information on the dynamical properties. Figure 2 tells us about the value of ρ on the (c,x)-plane, when the initial point to compute ρ is in $\mathrm{Fix}(S)$, i.e., of the form $(x,0)$. For the places in white the iteration of an initial point $(x,0)$, under HP_c, leads to escape. In particular, for $c{=}3/2$, for which value the E point has as eigenvalues $-1/2\pm \mathrm{i}\sqrt{3}/2$, all other points on the x-axis, with $x>-1$, escape (unless they belong to some stable manifold).

To compute ρ we have used a topological method based on the order of the iterates on the curve, see, e.g., the Appendix in [12]. The tolerance used to stop the computation of ρ is 10^{-10}. Then, if the value of ρ can be identified, with this tolerance, as a rational m/n with $n<10^4$, it is decided to consider $\rho\in\mathbb{Q}$ and, hence, they belong to islands with a period equal to the denominator. Otherwise we consider $\rho\notin\mathbb{Q}$. Points in light grey in Figure 2 are considered to have ρ irrational. Points with ρ of

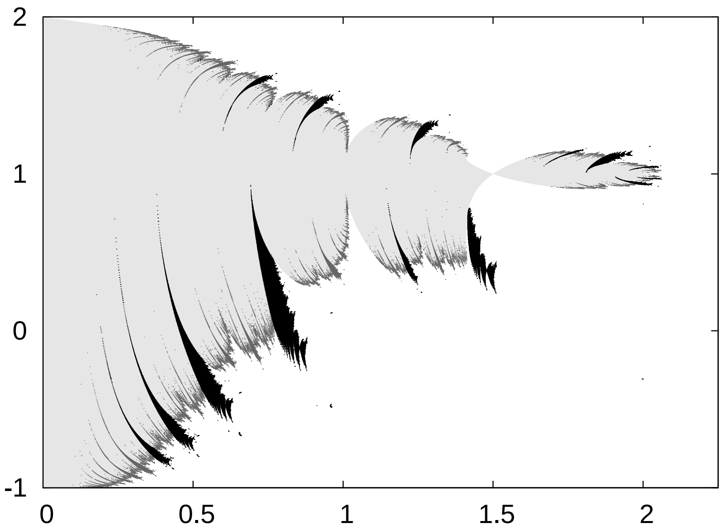

Figure 2: The plot shows, as a function of c (horizontal variable), the values of x (vertical variable) for points in $\mathrm{Fix}(S)$ for which ρ has been computed. The dots in light grey correspond to points for which there is good evidence that $\rho \notin \mathbb{Q}$, while for other points (in grey or black) a value $\rho \in \mathbb{Q}$ has been found. See the text for details.

the form m/n, with $n \in \{3, 5, 7, 9, 11\}$ are shown in black, while points with other rational values of ρ are shown in grey. The wedges in black, from left to right, have $\rho = 1/11, 1/9, 1/7, 2/11, 1/5, 2/9, 3/11, 2/7, 1/3, 4/11, 2/5, 3/7, 4/9$ and $5/11$, the last five showing up for $c > 3/2$. We note that all denominators are odd. A similar plot, but taking initial points in $\mathrm{Fix}(R)$ would give even values for n, see [13]. We also note that, in this plot, odd values of m appear in the lower part, while even values appear on the upper part.

We remark that most of the wedges associated with islands reach $x = 1$, but they are extremely narrow; below the pixel resolution. As rational numbers are dense, the light grey domains on the figure have, in fact, a Cantor-like structure. Furthermore, some of the island domains in the figure do not emerge from $x = 1$. They are related to satellites (and satellites of satellites, and so on) of the main islands. In some sense, the structure around each island and around its satellite islands repeats the structure of the full set, as a fractal object. This can be checked by magnifying the black domains in Figure 2.

2.2 Measure of the set of regular and chaotic confined orbits

In Figure 3 we show the measure, $\mu(c)$, of the set of bounded orbits as a function of c for the map HP_c, as given in (2). We should stress that there are many other more general conservative models (e.g., Hamiltonian systems with two or three degrees of freedom, such as the Restricted Three-Body Problem, or traveling waves of some PDE, such as the Michelson system [14, 15]) which have many features in common with what we display for the Hénon conservative map.

To produce Figure 3 we compute the Lyapunov maximal exponent, $\Lambda(p)$, for initial points p and for many values of c and a narrow grid of points. A typical spacing in the coordinates x and y for the grid is 0.0005. In most of the cases we first compute a transient of 10^6 iterates before starting to compute $\Lambda(p)$. In this way we detect most of the points which escape. A simple escaping criterion follows from the fact that if some forward iterate of p has x-component with $x < -1$, it will escape. A number of iterates

$m = 10^6$ is also used to produce an estimate of $\Lambda(p)$. If the value obtained is below 2×10^{-5}, the orbit of p is considered to be regular and, hence, bounded. Otherwise it is considered to be chaotic. In the latter case, we continue with additional iterations (up to 10^8 and in some cases up to 10^{10}) to check if we can consider the chaos as confined or if the orbit of p is finally escaping.

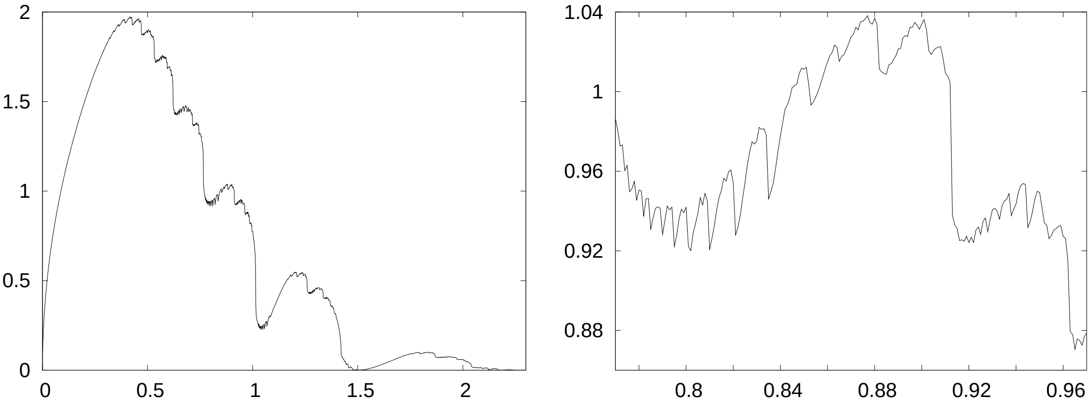

Figure 3: Left: measure $\mu(c)$ of the set of confined points as a function of c. Right: a magnification in the range $c \in [0.77, 0.97]$ to provide evidence of the self-similar properties of $\mu(c)$.

Note the sudden decrease of $\mu(c)$ at some values of c. Going from right to left one can see a first decrease near $c = 1.5$, a fact already mentioned in the discussion after Figure 2. The small confined area for $c = 1.5$ is due to the existence of tiny period-3 islands. Later on we see a sequence of sudden changes in $\mu(c)$ which correspond to the destruction of all the invariant curves surrounding the islands of periods 4, 5, 6 and so on.

The magnification shown in Figure 3, right, provides strong evidence of what happens with islands of a higher period and displays the self-similar properties of $\mu(c)$. As an example, the large jump near $c = 0.91$ corresponds to the breakdown of invariant curves around the islands of rotation number $2/9$, while the jump shortly after $c = 0.96$ corresponds to the breakdown of invariant curves around the islands of rotation number $3/13$. It is not difficult to identify all the jumps shown in these plots.

Among the points with bounded orbit there are, however, some which display chaotic behaviour. The Lyapunov exponent allows us to detect them. A natural question is, hence, how the measure of this set changes with the value of c. This is shown in Figure 4. The plot shows quite a sharp change in its behaviour. This is to be expected, because of the infinitely many chains of islands in the system (there are for any $\rho \in \mathbb{Q} \cap (0, 1/2]$). Each chain of islands has an associated hyperbolic periodic orbit, the splitting of whose invariant manifolds generates some amount of chaos. It is confined until the invariant curves, that surround these chaotic orbits, break down. Even considering that the computations shown in Figure 4 have been done with a 10^{-3} step in c, a careful examination of the data allows us to detect several hundreds of peaks. See Sections 2.3 and 2.4 for details on the splitting properties.

In Figure 5 we show three magnifications, computed with step 10^{-4} in c. They correspond to what happens before the breakdown of the invariant curves around the islands of periods 6, 5 and 4, respectively. For the moment, we do not consider the small jumps on these curves; just a kind of average or, better, a curve fitting the successive minima. For the left plot, for instance, this is produced by the change in the size of the chaotic zone created by the homoclinic points associated to the period-6 hyperbolic orbit. But

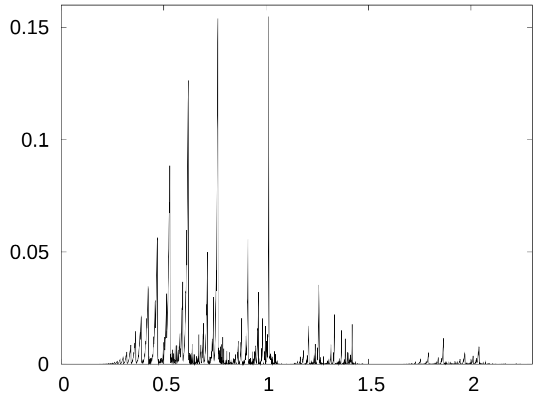

Figure 4: Measure of the set of confined points with chaotic dynamics as a function of c.

this orbit has been created at $c = c^0_{1/6} = 0.5$, while the destruction of all the invariant curves around the islands of rotation number $\rho = m/n = 1/6$ occurs for a critical value $c_{m/n} = c_{1/6} \approx 0.6204$. Hence, why does it take so long to see that the size of this zone is relevant? The answer will be give in Section 2.4. Similar things occur for the other two plots. The respective creation of islands and destruction of all the surrounding invariant curves occur, for period 5, at $c = c^0_{1/5} = 1 - \cos(2\pi/5) \approx 0.690983$ and $c = c_{1/5} \approx 0.7649$, and, for period 4, at $c = c^0_{1/4} = 1$ and $c = c_{1/4} \approx 1.0141$.

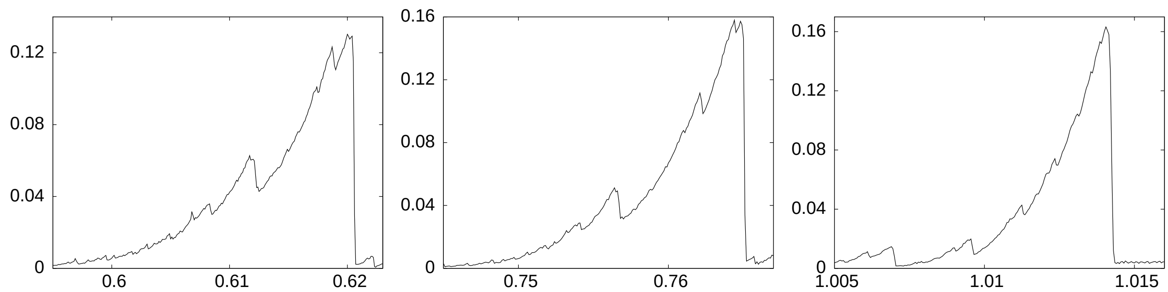

Figure 5: Magnification of Figure 4 corresponding to the breakdown of the invariant curves which surround the islands of period 6 (left), period 5 (centre) and period 4 (right).

The differences between an averaged behaviour of the rate of increase and the true behaviour in Figure 5 is due to the role of other minor islands. For instance, the jump seen in the left plot shortly after $c = 0.61$ corresponds exactly to the same kind of phenomenon, created by the periodic orbit of rotation number $\rho = 3/19$. The measure of the chaotic zone associated with this periodic orbit has to be added, in some sense, to the largest chaotic zone due to the period-6 orbit.

2.3 Splitting of the invariant manifolds of the hyperbolic fixed point

For their intrinsic interest and to compare with the behaviour in Section 2.4, we shall consider now a measure of the lack of coincidence of the unstable and stable manifolds, W^u_H, W^s_H of the hyperbolic fixed point. As a suitable measure we will use the splitting angle, that is, the angle between the manifolds, computed at the symmetric homoclinic point found on the first intersection with $y = 0, x > 1$. Let us denote the angle as $\sigma(c)$.

A useful parameter to present the results is $h(c)$, defined as follows. Let $\lambda(c)$ be the dominant eigenvalue at H, which is equal to $1+c+\sqrt{2c+c^2}$ for HP_c. Then we define $h(c)$ as $\log(\lambda(c))$. We note that $h(c)=\sqrt{2c}+\mathcal{O}(c)$. If in the limit vector field (3) we scale time by an additional factor $\sqrt{2}$ then the map HP_c will be well approximated by the $h(c)$-time map of (3). It is easy to check that the separatrix of the flow has the closest singularities to the real axis of the time, located at a distance $\tau=\pi$ of that axis. According to [16, 17], for any $\eta>0$, there exists $N(\eta)$ such that the splitting angle is bounded by $N(\eta)\exp(-2\pi(\tau-\eta)/h(c))$. This type of result is true for general analytic area preserving maps close to the identity map.

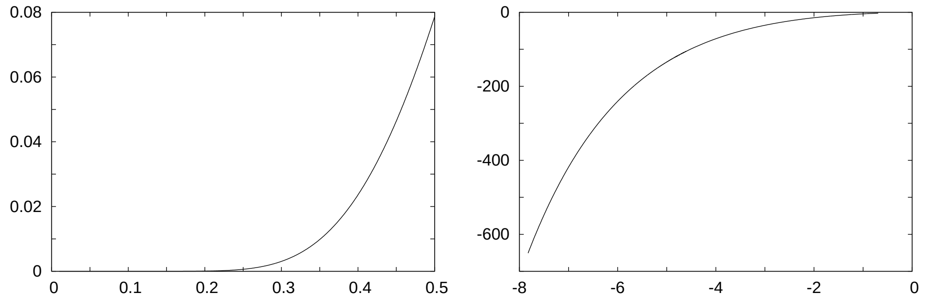

Figure 6: Different representations of the splitting angle $\sigma(c)$ between the manifolds at the first intersection with $y=0, x>1$. Left: σ as a function of c, showing that σ seems negligible for $c<0.2$. Right: $\log(\sigma)$ as a function of $\log(c)$, which allows to see how small $\sigma(c)$ is for c approaching zero.

For HP_c we have computed $\sigma(c)$ for many small values of c and the following formula fits the numerically computed data:

$$\sigma(c)=\frac{9}{2}\times 10^6\pi^2 h(c)^{-8}\exp\left(-\frac{2\pi^2}{h(c)}\right)\times\Omega(h), \tag{4}$$

the factor $\Omega(h)$, or correcting factor, being of the form $\omega_0+\mathcal{O}(h)$. Using a local representation of W_H^u to order 400 and 500 decimal digits in the computations it is possible to compute $\sigma(c)$ and, hence, to derive from (4) values of $\Omega(h)$ and to look for a formal expansion in powers of h^2: $\Omega(h)=\sum_{m\geq 0}\omega_{2m}h^{2m}$. See more details in [18, 19], but in contrast to [19], in the present case we have computed the splitting angle instead of the homoclinic invariant and derived the coefficients in $\Omega(h)$ using finite differences instead of polynomial fitting. The package PARI/GP [20] is useful for these simple problems.

As a result, the first digits of ω_0 are 2.48931280293671196250659825601239499970 46 and, furthermore, there is a strong numerical evidence that the formal series is, in fact, a divergent one. However, the related series $\sum_{m\geq 0}\omega_m h^{2m}/(2m)!$ (i.e., the Borel transform of $\Omega(h)$) seems to be convergent. In Figure 7, left, we plot $\log_{10}(\omega_{2m}(2\pi^2)^{2m}/(2m+6)!)$ as a function of m up to $m=375$, i.e., up to the power h^{750}. The values seem to tend to a constant, a strong evidence of the Gevrey-1 character of $\Omega(h)$ and of the fact that its Borel transform seems to have radius of convergence equal to $2\pi^2$. If we assume that, despite the divergent character of $\Omega(h)$, a good approximation is obtained for small h, if we truncate the expansion at the smallest term (in absolute value), the relative errors are shown in Figure 7, right. They are acceptably small, even for $h=1$.

If we compare the left plot in Figure 3 with Figure 5 we check that up to $c=0.35$ the behaviour of $\mu(c)$ just follows from the measure of the domain bounded by the separatrix

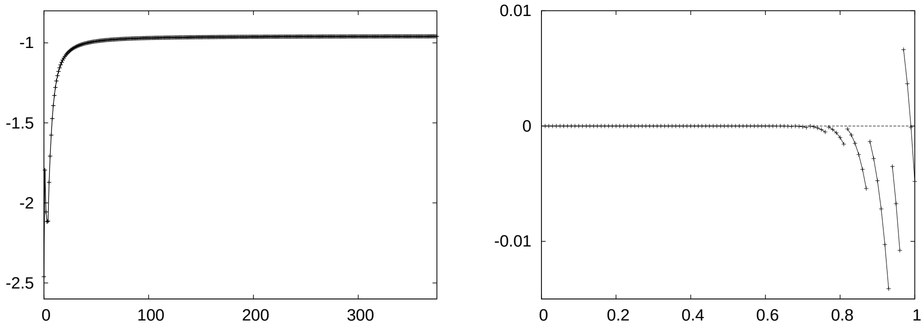

Figure 7: Left: $\log_{10}(\omega_{2m}(2\pi^2)^{2m}/(2m+6)!)$ as a function of m, which gives evidence of the Gevrey-1 character of $\Omega(h)$. Right: the relative errors $\Omega_{tr}(h)/\Omega(h) - 1$ as a function of h, with step 0.01, where $\Omega_{tr}(h)$ denotes the formal power series truncated at its smallest term, $m = m^*$. Note that this is achieved for different $m^* = m^*(h)$ depending on the value of h. The different pieces shown, from right to left, correspond to values of $m^*(h)$ equal to $4, 5, 6, \ldots$.

in Figure 1 and the change of scale. It is proportional to $\sqrt{c}$. No sign of the effect of the splitting seen on Figure 6 shows up. But this has to be expected, because all the points with chaotic orbits created by the splitting of $W_H^{u,s}$ escape to infinity. In contrast, Figure 8 displays, for the standard map in $\mathbb{T}^2$ (no escape), see (7), a comparison between the relative measure of the set of points with chaotic orbit (detected by computation of the Lyapunov exponent) and a multiple of the splitting angle of the manifolds of the hyperbolic fixed point, computed at the homoclinic point lying on the line $x = 1/2$. The agreement is good, even for large values of the parameter k in (7). In this formulation the Greene's critical value appears for $k \approx 0.15464$.

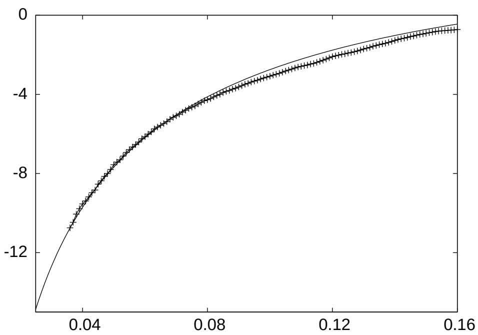

Figure 8: Fraction of points with chaotic orbit (line with points) and a multiple of the splitting angle of the hyperbolic fixed point for the standard map (continuous line). Horizontal variable: the parameter k, see (7). In the vertical line the natural logarithms of the values are displayed.

2.4 Splitting of the invariant manifolds of periodic hyperbolic points

Consider a map F having an elliptic fixed point E_0. Under generic conditions there is a domain of stability D surrounding E_0. Inside D the phase space has different Birkhoff resonant chains of islands of stability, located in an annular domain around E_0. Generically, these stability islands have a pendulum-like phase space structure formed by the invariant manifolds of the hyperbolic periodic points. Hence, for a concrete island, one can consider two "main" splittings of separatrices, geometrically related to the upper and lower separatrices of the classical pendulum. We refer to the inner/outer splittings according to the distance to E_0 of the separatrices of the pendulum structure. It turns out that both splittings are generically different, being the outer one the largest [11]. Hence, the size of the confined chaotic zone is expected to grow, essentially, proportionally to the outer splitting of the separatrices of the main chain of islands inside the stability domain.

In Figure 9 we show the behaviour of the outer splitting of separatrices of the islands with $\rho = 1/6$, $1/5$ and $1/4$ as the parameter c of the Hénon map (2) changes. Consider that the periodic orbit with rotation number ρ is created at the value $c = c_\rho^0$ (see Section 2.2). The fact that the invariant manifolds do not coincide creates a bounded chaotic region around the islands. However, the splitting of separatrices behaves in an exponentially small way in (maybe a power of) $\nu = c - c_\rho^0$. This means that the size of the splitting becomes large enough to be observable for relatively large values of ν. Then, the effect of the chaotic zone around the island of rotation number ρ contributes in a significant way to the total size of the confined chaotic region only for ν values for which the splitting can be observed. The Figure 9 shows the value of the splitting, for period 6, 5 and 4, from left to right, starting at the creation of the periodic island. Note the agreement with the Figure 5. The values of c at which the splitting starts to be seen in Figure 9 agree very well with the ranges shown in Figure 5.

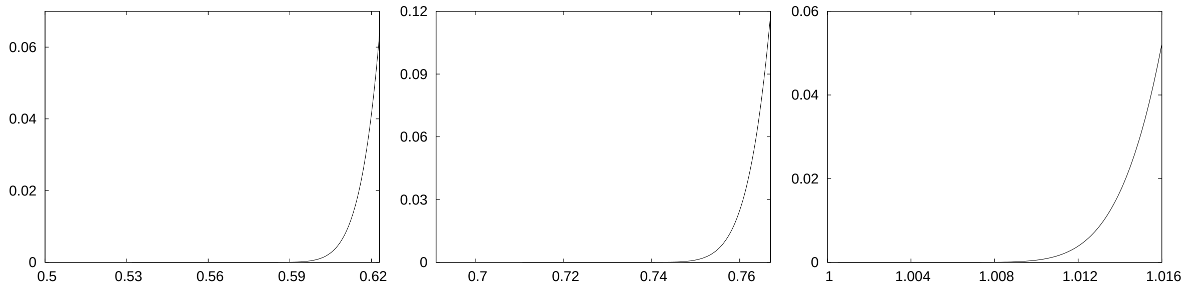

Figure 9: Behaviour of the outer splitting of the separatrices of the islands of period 6 (left), period 5 (centre) and period 4 (right). Compare with Figure 5.

The fact that the range in c, from the creation of the periodic islands of a given rotation number ρ, at $c = c_\rho^0$, till the destruction of the surrounding invariant curves, at $c = c_\rho$, becomes shorter when ρ increases (as observed in Figure 9 for $\rho = 1/6, 1/5$ and $1/4$) has an easy explanation. The islands travel "faster" across the confined domain around the point E because, when increasing c, the twist condition becomes weaker. A simple computation of the normal form around E shows that ρ changes from having the maximum at E to have a local minimum at E for $c = 5/4$.

2.5 The mechanism of destruction of invariant curves and the associated Cantor sets

The destruction of invariant curves can be seen, from an analytical point of view, as the lack of convergence of the sequence of iterations to obtain a conjugation between the dynamics on a candidate to be an invariant curve and a rigid rotation, with Diophantine rotation number, in $\mathbb{S}^1$, following the KAM approach (see e.g. [21]).

Another approach, from a geometrical point of view, is the obstruction method [22]. We will illustrate this last approach with an example. The invariant curves surrounding period-6 islands are destroyed for $c = c_{1/6} \approx 0.6204$, as said in Section 2.2. In Figure 10 some orbits are shown. The period-6 islands would be found to the right of the displayed orbits.

In the left plot, to improve visibility, we skip some of the invariant curves around the elliptic periodic orbits of rotation number 3/19 (with one point on $y = 0$) and 4/25 (without points on $y = 0$ in the displayed domain). Beyond many other chains of little islands, some invariant curves (according to the value of the rotation number, using the criterion explained in Section 2.1) are found passing close to the point $(-0.138, 0)$. In the right plot one can see again the islands of rotation numbers 3/19 and 4/25. Furthermore, the large dots on the plot show the location of some of the points in the related periodic hyperbolic orbits (with the same rotation numbers than the elliptic ones). We also show part of the manifolds of these hyperbolic periodic orbits. On the points shown the unstable manifolds leave the points with positive slope. It is easy to see that $W^u_{3/19}$ intersects $W^s_{4/25}$ (and, symmetrically, $W^s_{3/19}$ intersects $W^u_{4/25}$). Hence, due to these heteroclinic intersections, there is no room for invariant curves with $\rho \in (3/19, 4/25)$.

A description of the destruction of invariant curves can also be found in [23].

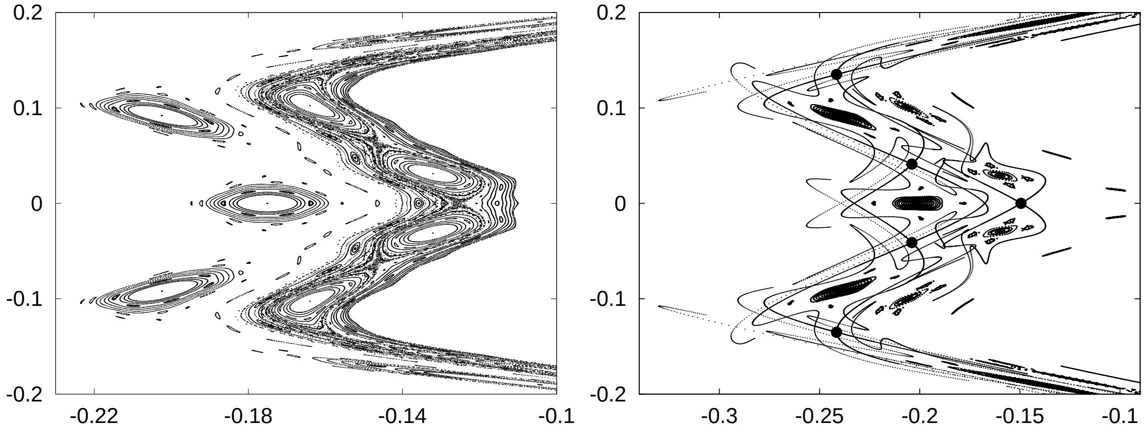

Figure 10: Several relevant orbits on the left part of the period-6 islands for values close to the destruction of the invariant curves around these islands. Left: Plot for $c = 0.618 < c_{1/6}$. Right: Plot for $c = 0.63 > c_{1/6}$. See the text for details.

It can seem strange that we must go to $c = 0.63$ to discover the existence of these heteroclinic intersections, while we claimed before that the destruction has been found for $c = c_{1/6} \approx 0.6204$. Plots similar to Figure 10, right, for $c = 0.625$ or $c = 0.628$ do not provide evidence of the existence of heteroclinic points. The reasons of this are simple:

1) The arc length of the part of the manifolds shown in the figure is short. Much longer parts will show heteroclinic points for values slightly larger than 0.6204.

2) Beyond the hyperbolic periodic orbits with $\rho = 3/19, 4/25$ there are infinitely many other hyperbolic periodic orbits with intermediate values of ρ. It would be possible to find a long chain of heteroclinic connections between the ones we consider here.

The "gaps" produced by the heteroclinic intersections on the candidate to invariant object are the responsible of the Cantor-like structure of these objects. Therefore, the points with chaotic dynamics that were confined when the invariant curve still existed, can escape when the curve is destroyed and it is replaced by a Cantor set. If the gaps of that set are rather small, however, it will take a long time for the iterates to find their way to escape.

2.6 Explaining the birth and death of islands

In the previous subsections we presented some elements which allow to have a fairly good understanding of the changes in the measure of the set of confined points under iteration by HP_c. We give here the main items concerning the fate of the islands.

1) For small values of c the map HP_c has a dynamics quite similar to the flow (3). The measure of the confined orbits is very close to the measure in the case of (3), scaled by $\sqrt{c}/2$. Periodic orbits of rotation number $\rho \in \mathbb{Q}$ and the corresponding islands are born at E for $c = c^0_\rho = 1 - \cos(2\pi\rho)$ and travel away from E when increasing c.

2) Simultaneously the hyperbolic periodic orbits with the same ρ go also away from E, the splitting $\sigma_\rho(c)$ of their manifolds creates first tiny chaotic domains which, later on, increase with c as $\sigma_\rho(c)$ increases. Finally the invariant curves surrounding the islands of a given ρ are destroyed due to the existence of heteroclinic intersections of the manifolds of hyperbolic periodic orbits of slightly smaller ρ and the confined chaotic domains can escape. The islands still exist for a while, until their central elliptic point becomes reflection hyperbolic.

3) For larger values of c the mechanism of creation of islands is different. The value of ρ at E is a local minimum for $c > 5/4$. Then, periodic orbits of a given ρ are created in pairs (two of elliptic type and two of hyperbolic type) near some place, away from E, close to a local maximum of the rotation number. This is related to the loss of the twist condition for a nearby integrable model and to the creation of the so-called meandering curves, see, e.g., [24]. When c increases, one of the periodic islands approaches E and the other approaches the boundary of the domain of confined orbits. As an example, for $\rho = 4/13$ the couple of periodic islands is created for $c \approx 1.345$. One of them ends at E for $c \approx 1.3546$, while the other has surrounding invariant curves until $c \approx 1.369$ and, finally, the island is destroyed near $c = 1.391$.

To see the evolution of the set of confined orbits as a function of c, details on the evolution of an island and on the changes in the set of chaotic confined orbits the reader can have a look at some movies, available in `http://www.maia.ub.es/dsg/QuadraticAPM`.

3 The Hénon conservative orientation-reversing map

For our purposes, to study the islands in the standard map, it is also relevant to consider the Hénon conservative map, but with orientation-reversing, HR_c, which is given (using a setting similar to the one in (2)) by

$$HR_c \begin{pmatrix} x \\ y \end{pmatrix} \to \begin{pmatrix} x + \frac{c}{2}(1-(x-y)^2) \\ -y - \frac{c}{2}(1-(x-y)^2) \end{pmatrix}, \tag{5}$$

where, again, it is enough to consider $c > 0$. We name it HR which stands for Hénon conservative-reversing map. It has two fixed points, $H_\pm$, located at $(\pm 1, 0)$, hyperbolic for all c. Because of the orientation-reversing character, they have a positive and a negative eigenvalue, given by $\lambda^u_\pm = \mp c \mp \sqrt{c^2+1}$, $\lambda^s_\pm = \mp c \pm \sqrt{c^2+1}$. Note that the absolute value of the unstable eigenvalues, coincides. Furthermore, it has a period-2 periodic orbit, whose points $E_\pm$ are located at $(0, \pm 1)$. They are elliptic for $c \in (0, 1)$, with limit rotation number $\rho(c) = \cos^{-1}(1-2c^2)/(2\pi)$, parabolic for $c = 1$ and reflection hyperbolic for $c > 1$.

The map HR_c has a reversor $\hat{S}$, defined by $\hat{S}(x, y) = (-x, y)$ and, hence, an additional reversor $\hat{R} = \hat{S} \circ HR_c$. Both of them are involutions and satisfy similar properties to the HP_c case. In particular $\hat{S} \circ HR_c \circ \hat{S} = HR_c^{-1}$, quite useful to obtain stable manifolds from unstable ones.

The square of the map can be approximated by a limit flow. No scaling of the variables is needed now. Only a scaling of time by a factor $2c$. The reason to select this scaling will be given later. Letting c go to zero we obtain the limit flow

$$\frac{dx}{dt} = \frac{1}{2}(1 - x^2 - y^2), \quad \frac{dy}{dt} = xy, \tag{6}$$

whose Hamiltonian is $H = y(1 - x^2 - y^2/3)/2$. The separatrices are given by $y = 0$ and $1 - x^2 - y^2/3 = 0$. It is immediate to check that the separatrix going from $x = -1$ to $x = 1$ on $y = 0$ has a singularity for $t = \mathrm{i}\pi$, while the other separatrices, upper and lower, going from $(1, 0)$ to $(-1, 0)$ along $x^2 + y^2/3 = 1$, with extremal values $|y| = \sqrt{3}$, have singularities for $t = \mathrm{i}\pi/2$. The Figure 11 shows the flow of (6) and several iterates of HR_c for $c = 0.2$. In the right part of the figure, the upper points (on top of what seems to be a connection between the saddles, close to $y = 0$) are mapped by HR_c to the lower ones, and reciprocally. As in the case of HP_c, shown in Figure 1, for small c the dynamics of the map is rather close to the one of the flow. No trace of chaotic behaviour is seen at the resolution level of the plot.

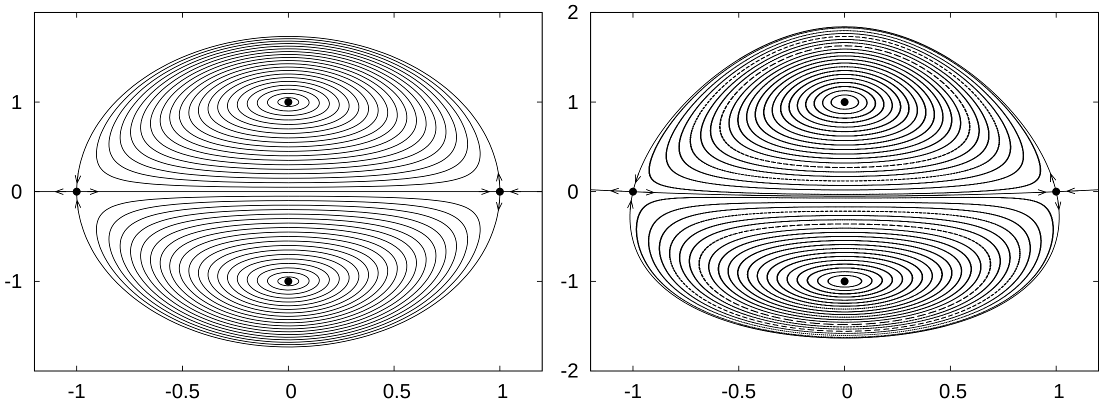

Figure 11: Left: Phase portrait of the limit flow given by (6). Right: Some orbits of HR_c for $c = 0.2$, which seem to correspond to an integrable map. The invariant manifolds of the hyperbolic fixed points $H_\pm$ seem to be coincident.

However, there exist transversal heteroclinic points in $W^u_{H_-} \cap W^s_{H_+}$ (near the line $y = 0$) and in the upper and lower branches of $W^u_{H_+} \cap W^s_{H_-}$. Due to the symmetry $\hat{S}$ it is easy to locate these points on $x = 0$. In Figure 12 we use as parameter $h(c) = \log((\lambda^u_-)^2) = 2\log(c + \sqrt{c^2+1}) = 2c + \mathcal{O}(c^2)$. The reason to use the square is the fact that we are doing the computations with the map HR_c^2. Furthermore, the fact that the dominant term in $h(c)$ is $2c$ is what justifies the time scaling done to obtain (6).

The splitting of the invariant manifolds has been measured by computing the splitting angle $\sigma(c)$ on $x = 0$, both at the heteroclinic point in $W^u_{H_-} \cap W^s_{H_+}$, that we denote as $\sigma_0(c)$, and at the one in the upper branches of $W^u_{H_+} \cap W^s_{H_-}$, that we denote as $\sigma_+(c)$. Assuming a behaviour similar to the one in (4), i.e., of the form $\sigma(h) = Ah^B \exp(-C/h)(1 + \mathcal{O}(h))$,

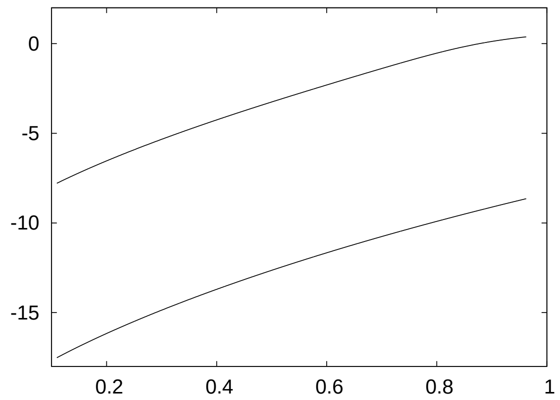

Figure 12: Values of the splitting angle for the separatrices in the case of HR_c. Here we plot $\log(\sigma(c))h(c)$ as a function of $h(c)$. The upper curve corresponds to the separatrix in the upper part of Figure 11, right, and the lower one to the separatrix near $y = 0$. For the separatrix in the lower part of Figure 11, right, the values are close to the ones in the upper part. See the text for details.

for suitable constants A, B, C, suggests to plot $\log(\sigma(c))h(c)$ as a function of $h(c)$. This is done in Figure 12, the upper curve corresponding to $\sigma_+(c)$ and the lower one to $\sigma_0(c)$. A fit of the data gives values for the constant C in the exponential term which clearly tend to π^2 and $2\pi^2$, when the data used are restricted to domains in the left part of the plot (i.e., smaller values of $h(c)$). This is in perfect agreement with the location of the singularities of the separatrices of the vector field in (6).

Finally, as we did in the HP_c case in Section 2.2, we plot a measure of the set of confined points as a function of c in Figure 13. One can check that the limit value, for $c \to 0$, is $\pi\sqrt{3}$, in agreement with the flow case in Figure 11, left. For $c = \sqrt{3}/2$, corresponding to elliptic fixed points with limit rotation number 1/3, the measure goes to zero. It is easy to detect jumps near $c = 0.709, 0.608, 0.538, 0.487, \ldots$, corresponding to the destruction of invariant curves surrounding the islands of period $4, 5, 6, 7, \ldots$, respectively, under HR_c^2, both in the upper and lower part.

The behaviour of the measure of the set of confined chaotic points, the mechanism of destruction of invariant curves, etc, under the map HR_c^2 are similar to the ones described for HP_c.

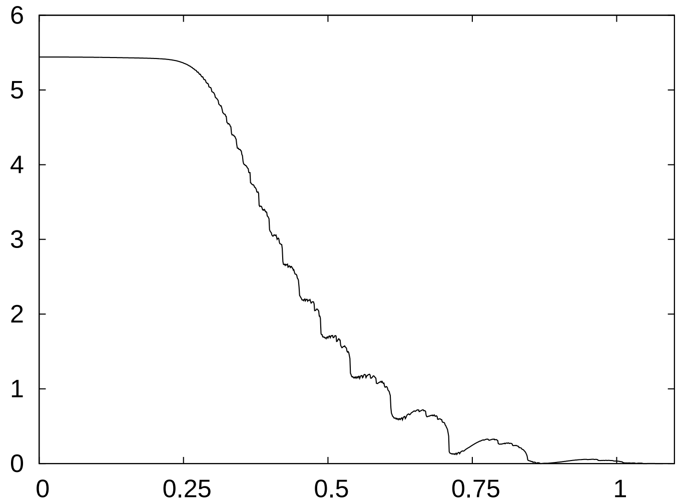

Figure 13: Measure of the set of confined points for HR_c as a function of c.

4 The standard map for large parameter values

In this Section we consider Chirikov's standard map [8]:

$$M_k : \begin{pmatrix} x \\ y \end{pmatrix} \to \begin{pmatrix} \bar{x} \\ \bar{y} \end{pmatrix} = \begin{pmatrix} x + \bar{y} \\ y + k\sin(2\pi x) \end{pmatrix}, \tag{7}$$

defined on the unit torus $\mathbb{T}^2 = \mathbb{S}^1 \times \mathbb{S}^1$. Here k is a distance-to-integrable parameter [25]: for $k = 0$ the phase space is foliated by horizontal invariant curves and the chaotic zone becomes visible as k increases. A remarkable value of the parameter k is Greene's threshold, $k \approx k_G = 0.971635\ldots/(2\pi)$, at which the last rotational invariant curves (the ones with $g = (\sqrt{5}-1)/2$ and $1-g$ as rotation numbers) is critical. Hence, for $k > k_G$ the motion in the y variable can be unbounded.

For large enough values of k one would expect the chaotic sea to fill the whole phase space. When dealing with the problem of the relative measure of the stochastic zone, Chirikov and Izraelev in [26] and [8] proved the existence of some special stable fixed points and 2-periodic orbits in the torus $\mathbb{T}^2$ appearing near integer values of k, named by them as *islets of stability*. They also suggested that such orbits should scale both in area as $1/k^2$ and in the range of the parameter where they existed as $1/k$.

In Section 4.1 we give numerical evidence of the fact that these islets appear to be the largest islands in the phase space for large enough k, and that such scalings hold. Moreover, a similar structure is observed near half-integer values of the parameter, with similar scaling properties.

4.1 Measure of the set of regular points

In order to detect any regular area in the phase space of the standard map M_k, we have computed on a fine grid (typically with step 5×10^{-5} both in x and y) the measure of the set of points in the phase space which are regular, the ones for which we can consider the Lyapunov exponent to be zero [27] as a function of the parameter k, say $A_r(k)$. Note that it is a lower bound on the total regular area, since one could find other islands, islands below the pixel size, or even below the machine precision used. See [28] and [29].

In Figure 14 one can see the regular area of M_k as a function of k in the range $k \in [1.75, 10.75]$. In this figure one observes that the area seems to vanish everywhere but near integer and half-integer values of k, where some peaks show up. Moreover, the non-vanishing area seems to decrease as a negative power of k. The same seems to happen concerning the range in the parameter where these peaks appear.

In fact, it is easy to check that M_k has, when considered on $\mathbb{T}^2$, the following remarkable orbits:

- If $k = n \in \mathbb{Z}$ it has 4 fixed points on the line $y = 0$: $x = 0, 1/2$ are hyperbolic and reflection hyperbolic respectively, and $x = 1/4, 3/4$ are unstable parabolic. In fact they are on an elliptic-hyperbolic (EH) bifurcation, where a fixed hyperbolic and a fixed elliptic point are born. These four fixed points and the two which are born at integer values of k lie on $y = 0$ as k varies. It also has a 2-periodic parabolic orbit at $(1/4, 1/2) \leftrightarrow (3/4, 1/2)$ at a period-doubling (PD) bifurcation. These points lie on symmetry lines of M_k (see [30]), $y = 2x$ and $y = 2x - 1$ respectively.

  Let us denote these points as $p_1^1 = (1/4, 0)$, $p_1^2 = (3/4, 0)$ and $p_2 = (1/4, 1/2)$ when dealing with k near integer. The subscript denotes the period.

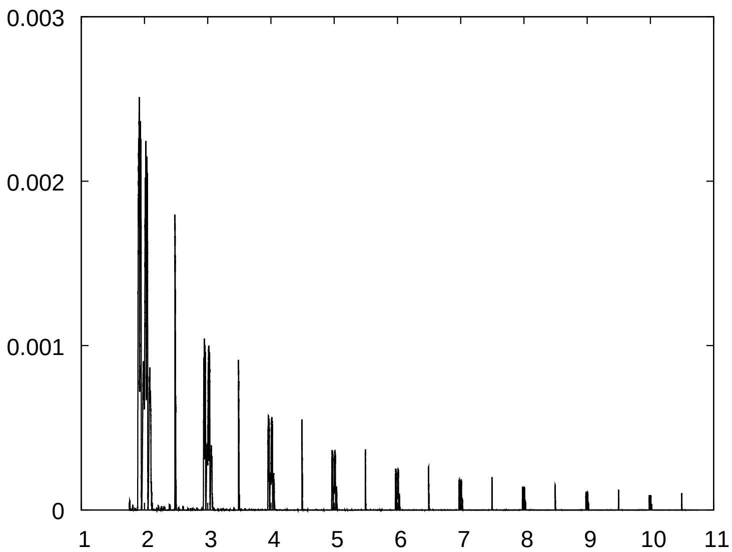

Figure 14: Relative measure $A_r(k)$ in the phase space of M_k of the number of points with zero Lyapunov exponent as a function of the parameter $k = 1.75(0.00005)10.75$.

- If $k = m + 1/2$, $m \in \mathbb{Z}$ the map M_k has a parabolic 4-periodic orbit at a PD bifurcation $(1/4, 1/2) \to (1/4, 0) \to (3/4, 1/2) \to (3/4, 0)$. The points on $y = 1/2$ lie on $y = 2x$ as k evolves, and the other two points remain on $y = 0$.

  Let us denote $p_4 = (1/4, 1/2)$ when dealing with k near to half-integer. Again the subscript denotes the period.

Remark 1. *Near half-integer values of k, there is another stable 4-periodic orbit of M_k near p_4, but contrary to this last, its position in the phase space depends on the value of k. In Section 5.1 we are going to justify that, due to a symmetry, the structure and evolution of such orbit can be obtained directly from the study of the dynamics around p_4.*

Concerning the parameter, numerical continuation of some of these orbits suggests that the range in k where the islands evolves scales as $1/k$, as predicted by Chirikov [8]. Namely,

- the island around p_2 is born at $k \approx n - 2/(n\pi^2)$, in an EH bifurcation, and passes through PD at $k = n$, $n \in \mathbb{Z}$,
- the islands of $p_1^{1,2}$ are born simultaneously at $k = n$ and have their PD at $k \approx n + 2/(n\pi^2)$, $n \in \mathbb{Z}$, and
- all islands of the orbit of p_4 are born at $k \approx m + 1/2 - 1/(2\pi^2(m + 1/2))$ where they have a degenerate saddle-centre bifurcation (see [29]), also referred as '0–4'-bifurcation in [7]), and have their PD at $k = m + 1/2$, $m \in \mathbb{Z}$.

In Figure 15 we have plotted magnifications near such values and we have superimposed them scaled as we have just suggested: we have plotted $n^2 A_r(k)$ as a function of $n(k - n)$, where n is integer or half-integer. These plots show that these islands scale as predicted, and the larger is k, the better these scalings fit. This suggest the existence of a limit behaviour for $k \to \infty$, which is the contents of Section 5.

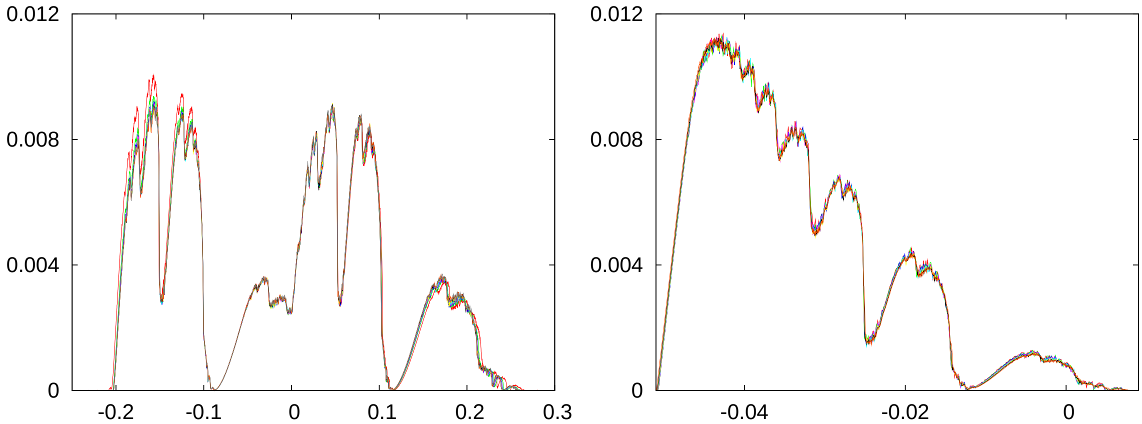

Figure 15: Superimposed scaled areas $n^2 A_r(k)$ as a function of the scaled parameter $n(k-n)$ near: Left: $n = 2, 3, \ldots, 10$. Right: $n = 2.5, 3.5, \ldots, 10.5$.

In the left plot in Figure 15 one can see that the fixed points and the 2-periodic orbit coexist in some range of the parameter close to integer, and that the evolution seems to repeat. This is to be clarified in Section 5.1. Moreover, a rougher version of each of them was previously computed by Karney et al. in [9], where the author studies the effect of these islands in the overall diffusion of the standard map in the presence of noise.

5 Relating the islands in the standard map to the Hénon map

The numerical results of the previous section suggest that the islands appearing near each integer and half-integer value of k for M_k (7) scale in the x and y variables, and in the range of the parameter k where they subsist as $1/k$, and that this scaling becomes more exact as k increases. In contrast with usual cases where the limit map is derived from a return map including a passage of the orbits near a homoclinic tangency, see, e.g., [1], now it is obtained directly: no points of the relevant orbits come close to any saddle of the initial map.

In Section 5.1 we prove the existence of a limit behaviour of the dynamics around $p_1^{1,2}, p_2$ and p_4 as $k \to \infty$, and that such limits are, in fact, Hénon maps with a suitable reparametrisation. In Section 5.2 we compare the numerical results for the Hénon map given in Sections 2.2 and 3 and the ones in Section 4.1 for the standard map, using the scalings of Proposition 1. Finally, in Section 5.3 we give evidence of the role of the islets in the overall diffusion properties of the standard map via the one-step diffusion coefficient.

5.1 Theoretical results

The contents of this subsection is summarized in the following

Proposition 1. *There exist a limit behaviour of the dynamics around $p_1^{1,2}$ and p_2 (resp. p_4) under scalings in x, y and k by $1/n$ for $n \in \mathbb{Z}$ (resp. $n - 0.5 \in \mathbb{Z}$). Moreover, these limit maps are conjugated to area preserving orientation-preserving (resp.-reversing) Hénon maps, depending on a suitably scaled parameter.*

Proof of proposition 1 part I: Limit maps

In this subsection we derive limit maps for the dynamics around $p_1^{1,2}, p_2$ and p_4 by means of expanding a suitably scaled M_k^ν in Taylor series around each p_ν, where ν denotes its period. The symmetries of the standard map are used to reduce computations and to simplify the limit maps, but in any case one can obtain them without its aid. Let us introduce

$$E : \begin{pmatrix} x \\ y \end{pmatrix} \mapsto \begin{pmatrix} n^* x \\ n^* y \end{pmatrix},$$

where we will set $n^* = n \in \mathbb{Z}$ for $\nu = 1, 2$ and $n^* = m + 1/2, m \in \mathbb{Z}$ for $\nu = 4$. Consider also the translation and central symmetry

$$T_{(x_0,y_0)} : \begin{pmatrix} x \\ y \end{pmatrix} \mapsto \begin{pmatrix} x - x_0 \\ y - y_0 \end{pmatrix}, \quad S : \begin{pmatrix} x \\ y \end{pmatrix} \mapsto \begin{pmatrix} -x \\ -y \end{pmatrix}.$$

Let us start with k close to $n \in \mathbb{Z}$ and set $n^* = n$. Consider a new parameter $k' = n(k - n)$, which controls the scaled distance to the nearest integer

1. Near $p_1^1 = (1/4, 0)$, consider the change of variables

$$L_1 = E \circ T_{(1/4,0)} \circ M_k \circ T_{(1/4,0)}^{-1} \circ E^{-1}.$$

This gives

$$\begin{aligned} \begin{pmatrix} x \\ y \end{pmatrix} &\overset{\text{(i)}}{\mapsto} \begin{pmatrix} x/n + 1/4 \\ y/n + 1/2 \end{pmatrix} \\ &\overset{\text{(ii)}}{\mapsto} \begin{pmatrix} 3/4 + (x+y)/n + (k/n + n)\sin(2\pi(x/n + 1/4)) \\ 1/2 + y/n + (k/n + n)\sin(2\pi(x/n + 1/4)) \end{pmatrix} \\ &= \begin{pmatrix} 1/4 + (x + y + k - 2\pi^2 x^2)/n \\ (y + k - 2\pi^2 x^2)/n \end{pmatrix} + \mathcal{O}(n^{-3}) \\ &\overset{\text{(iii)}}{\mapsto} \begin{pmatrix} x + y + k - 2\pi^2 x^2 \\ y + k - 2\pi^2 x^2 \end{pmatrix} + \mathcal{O}(n^{-2}), \end{aligned}$$

where (i) is the map $T_{(1/4,0)}^{-1} \circ E^{-1}$, (ii) corresponds to M_k and (iii) is the map $E \circ T_{(1/4,0)}$. Then, near p_1 and for k near integer we have the following behaviour:

$$L_1 : \begin{pmatrix} x \\ y \end{pmatrix} \mapsto \begin{pmatrix} \bar{x} \\ \bar{y} \end{pmatrix} = \begin{pmatrix} x + \bar{y} \\ y + k' - 2\pi^2 x^2 \end{pmatrix} + \mathcal{O}(n^{-2}). \tag{8}$$

The map around p_1^2 is the same as L_1, but composed with S.

2. Near $p_2 = (1/4, 1/2)$, if we perform the following change of variables

$$L_2 = E \circ T_{(1/4,1/2)} \circ S \circ M_k \circ T_{(1/4,1/2)}^{-1} \circ E^{-1}$$

we obtain

$$L_2 : \begin{pmatrix} x \\ y \end{pmatrix} \mapsto \begin{pmatrix} \bar{x} \\ \bar{y} \end{pmatrix} = \begin{pmatrix} -x + \bar{y} \\ -y - k' + 2\pi^2 x^2 \end{pmatrix} + \mathcal{O}(n^{-2}). \tag{9}$$

Here we have taken $S \circ M_k$ instead of M_k^2. This fact allows us to deal with a quadratic map instead of a quartic one. To obtain this expression one has to mimic the previous computation of L_1.

Now consider $n^* = m + 1/2, m \in \mathbb{Z}$. Here $k' = (m + 1/2)(k - m - 1/2)$ is the new parameter to be used.

3. Near $p_4 = (1/4, 1/2)$, the change of variables

$$L_4 = E \circ T_{(1/4,1/2)} \circ S \circ M_k^2 \circ T_{(1/4,1/2)}^{-1} \circ E^{-1}$$

gives

$$L_2 : \begin{pmatrix} x \\ y \end{pmatrix} \mapsto \begin{pmatrix} \bar{x} \\ \bar{y} \end{pmatrix} = \begin{pmatrix} -x - y - s_0 + \bar{y} \\ -y - s_0 - s_1 \end{pmatrix} + \mathcal{O}(n^{-2}), \tag{10}$$

where $s_0 = k' - 2\pi^2 x^2$ and $s_1 = k' - 2\pi^2(x + y + s_0)^2$. Here we have also used $S \circ M_k^2$ instead of M_k^4. This allows to reduce the degree of the limit map from 16 to 4.

Proof of proposition 1 part II: L_1, L_2 and L_4 are Hénon maps

To find the conjugacies which relate our limit maps to a Hénon map HP_c or HR_c we shall just move their symmetry lines to $y = 0$ for HP_c and to $x = 0$ for HR_c, and to make the position in the phase space of some particular orbits not to depend on the parameter. After these changes, a new parameter is going to be defined, plus some scalings in the (x, y)-variables, which coincide in all cases and depend on the new parameter. The results in Table 1 summarize the suitable scalings and reparametrisations.

Map	Sym. line	Hénon map	New parameter	Scaling
L_1	$y = 0$	HP_c	$c = \sqrt{2}\sqrt{k' + 2/\pi^2}$	$2\pi/c$
L_2	$y = 2x$	HP_c	$c = \sqrt{2}\sqrt{2 + k'\pi^2}$	$2\pi^2/c$
L_4	$y = 2x$	$(HR_c)^2$	$c = \sqrt{1 + 2k'\pi^2}$	$2\sqrt{2}\pi^2/c$

Table 1: Hénon maps to which L_1, L_2 and L_4 are conjugated. The new parameter and scalings in x and y are given in the last two columns.

Concerning the second 4-periodic orbit near p_4 (see Remark 1), it corresponds to the 2-periodic orbit of the orientation-reversing Hénon map HR_c. Such 4-periodic orbit can be found on the symmetry lines of M_k, $\{y = 2x\} \to \{y = 0\} \to \{y = 2x - 1\} \to \{y = 0\}$. Its position depends on the value of the parameter, but its distance to the 4-periodic orbit of p_4 scales as $1/k$ in distance measured on the symmetry lines.

With these results, up to terms of the order of $1/k^2$ for both integer and semi-integer values of the parameter, the scalings predicted by Chirikov and Izraelev in [26] and [8] are fully justified. Moreover, since the bifurcations of fixed points of conservative Hénon maps are well known, this allows to identify, up to some controlled error, the bifurcations of the orbits of $p_1^{1,2}$, p_2 and p_4.

This ends the proof of Proposition 1.

Remark 2. *Karney et al. in [9] used the fact that the fixed point* $p_1^{1,2}$ *was in its EH-bifurcation to derive an approximate mapping to describe its dynamics, which they truncated at order 2. In this paper the authors also give the relation of such a map with* HP_c*, and give the scalings for* L_1 *as in Table 1, but there is no justification for the suppression of higher order terms in the limit* $k \to \infty$.

Remark 3. *The same procedure applies exactly for Zaslavsky's web map [31] whose most studied version is the so-called four-fold web map, which has the form*

$$W_k : \begin{pmatrix} x \\ y \end{pmatrix} \mapsto \begin{pmatrix} \bar{x} \\ \bar{y} \end{pmatrix} = \begin{pmatrix} y \\ -x - k\sin(2\pi y) \end{pmatrix}. \tag{11}$$

Here again, we consider (11) in the torus $\mathbb{T}^2$*. For values of k near an integer there are two fixed points at* $(1/4, 1/4)$ *and* $(3/4, 3/4)$ *and a 2-periodic orbit* $(1/4, 3/4) \leftrightarrow (3/4, 1/4)$*, and for k near a half-integer, there is a 4-periodic orbit* $(1/4, 1/4) \mapsto (1/4, 3/4) \mapsto (3/4, 3/4) \mapsto (3/4, 1/4)$*. Again, the dynamics around these orbits near integer and half-integer values of k is a quadratic area-preserving Hénon map, which can be easily found with the aid of the symmetries of this map,* $y = x$ *and* $y = -x$ *and using exactly the same scalings as in Proposition 1.*

Remark 4. *Far from the separatrix, by setting* $y = y_0 + s$, $y_0 >> 1$ *in the separatrix map model*

$$SM_{a,b} : \begin{pmatrix} x \\ y \end{pmatrix} \mapsto \begin{pmatrix} \bar{x} \\ \bar{y} \end{pmatrix} = \begin{pmatrix} x + a + b\log|\bar{y}| \\ y + \sin(2\pi x) \end{pmatrix}, \tag{12}$$

the standard map (7) is recovered, depending on $k = b/|y_0|$*, with an error* $\mathcal{O}(y_0^{-2})$ *(see [25]). The 2-periodic and 4-periodic stable islands of this section appear in the phase space of* $SM_{a,b}$ *for b large enough (then the* $SM_{a,b}$ *is a good model of a close to integrable area-preserving map F, provided* b/y_0^2 *is small enough), see [29]. In particular the 4-periodic islet was shown to be born at a degenerate saddle-centre bifurcation.*

We also would like to note that in [32], both accelerator modes and ballistic modes are studied for the standard map and for the models in (11) and (12) related to the fixed and period-2 points.

5.2 Comparing numerical results

Proposition 1 tells us that the limit maps around $p_1^{1,2}$, p_2 and p_4 are Hénon maps except for a controllable error. With the aid of the data in Table 1 we can recover the plots of the scaled regular area for the standard map as a function of the scaled parameter from the numerical study we did for the Hénon maps in Sections 2.2 and 3. This is the contents of Figure 16.

From the expression of the limit maps L_1 (8) and L_2 (9) one can easily see that the relative regular area around the elliptic fixed point is the same, but shifted in the parameter. We have plotted the corresponding scaled relative regular area for both limit maps in Figure 16, bottom left. Note further that to recover the actual relative regular area (non-scaled) as in Figure 14 one has also to take into account that near integer values of the parameter there are two fixed points p_1^1 and p_1^2 and that p_2 is 2-periodic. Near half-integer values of the parameter there are two 4-periodic islands.

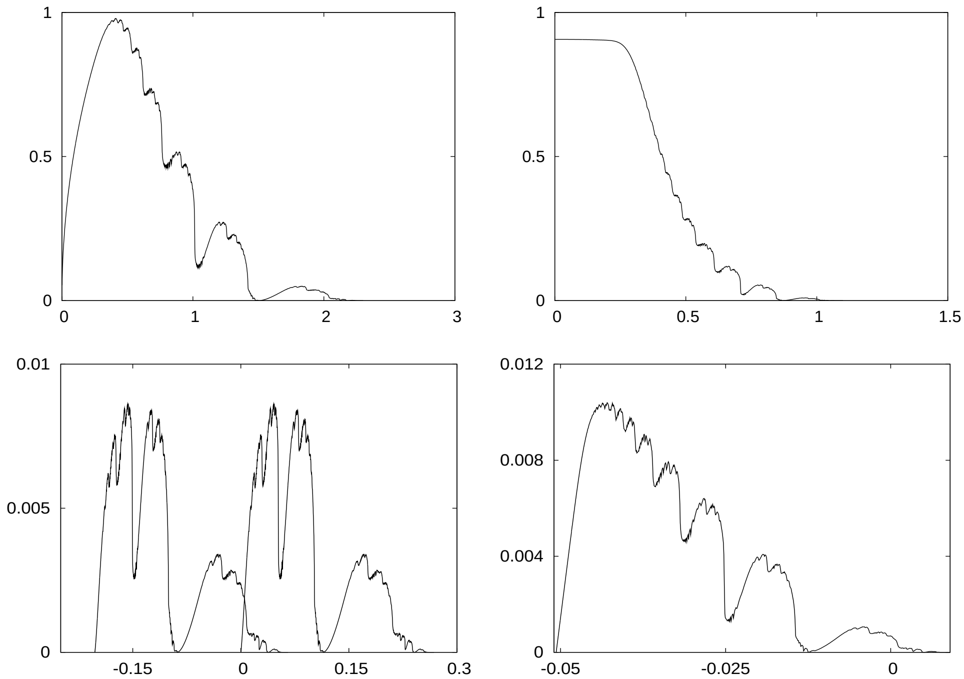

Figure 16: Evolution of the relative regular area of: Top: Left: HP_c, Right: HR_c. Bottom: Left: L_1, L_2 Right: L_4. These last two figures are obtained from the evolution of the non-escaping points of the area preserving Hénon maps plus the scalings in Table 1.

5.3 A preliminary study of the diffusion properties

For large values of k, at least $2/\pi$ in our setting (where the elliptic fixed point at $(x, y) = (0.5, 0)$ becomes unstable), the statistical description of the dynamics in the chaotic zone (here it is required that the regular zone is negligible in front of the chaotic zone) can be done via the simplest diffusional equation [33]

$$\frac{\partial f}{\partial t} = \frac{1}{2} D_k \frac{\partial^2 f}{\partial y^2}.$$

Here $f = f(y, t)$ where t denotes the number of iterates and y is the momentum. Note that here the angles x are averaged out. The average diffusion rate for M_k, D_k, can be evaluated as the limit

$$D_k = \lim_{n\to\infty} \frac{\langle(\Delta y)^2\rangle}{n}, \tag{13}$$

which, under the assumption that one could average with respect to the angle and that the effect of the islands is negligible, takes the value

$$D_{ql} = \frac{k^2}{2}, \tag{14}$$

a value which is referred to as the quasi-linear value. The symbol Δy denotes the difference in momentum between two consecutive iterates of the map and $\langle\cdot\rangle$ denotes ensemble average.

Chirikov in [8] performed extensive numerical simulations to evaluate such rate, and found the behaviour predicted in (13) plus fluctuations, for which he suggested the islets of stability as responsible for that.

To investigate the role of the islets of stability, in this simple approximation, we have evaluated (13) (meaning the variance of the change of momentum per iterate) for the standard map in an ensemble of points that fills, in an approximately uniform way, the complement in the torus of the islets, using the following procedure:

1. Compute an approximation of the right branch of the unstable invariant manifold of the origin W^u_+, via any available method. In this case the results do not depend on this choice.

2. Compute a fundamental domain U where the approximated expression of W^u_+ differs from the original map less than a prefixed tolerance.

3. Choose points in U and iterate them for a transient of n_0 iterates. This will fill, in a reasonable uniform way, the whole chaotic area.

In our computations, we have used the well-known *parametrisation method* (see [27]) at order 10, with a tolerance 10^{-20} in our fundamental domain. Our transient was $n_0 = 10^3$, and we have performed $n = 10^6$ iterates per each of the $m = 10^5$ initial conditions we took. The results can be seen on Figure 17. No change in the results is observed if different values are used for n_0, n or m. The results also coincide if the unstable invariant manifold of a 2-periodic hyperbolic point is used instead of W^u_+.

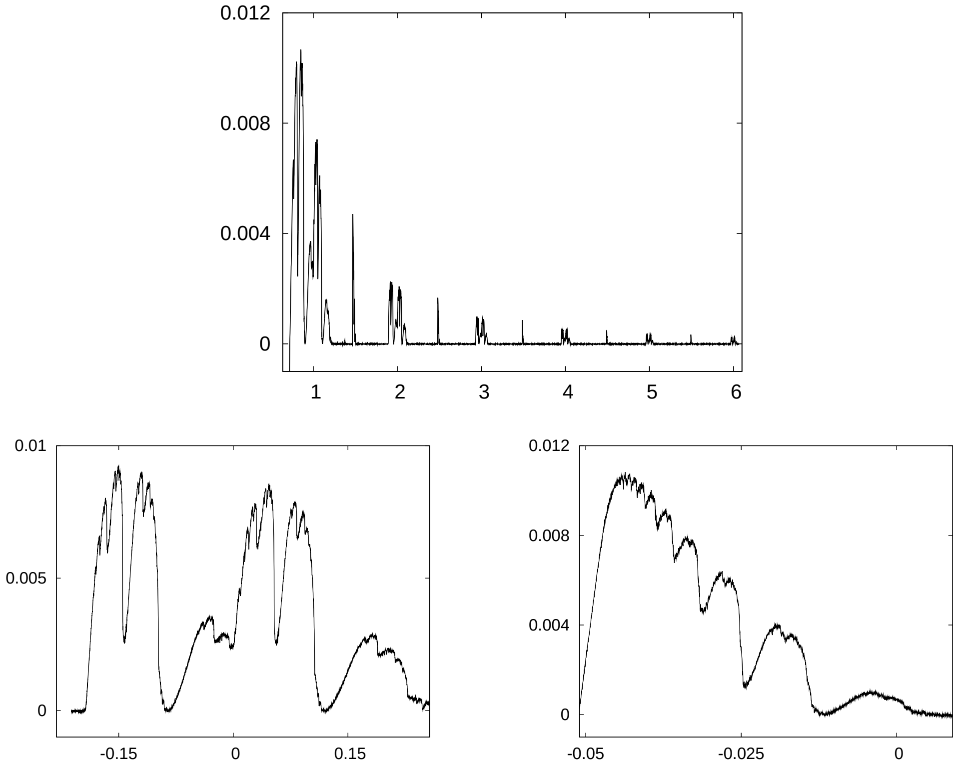

Figure 17: Left: Diffusion coefficient D_k/D_{ql} normalised to the quasi-linear value and turned upside down: $1 - D_k/D_{ql}$. Centre: Magnification near $k = 2$ of $1 - D_k/D_{ql}$, scaled. Right: Magnification near $k = 2.5$ of $1 - D_k/D_{ql}$, scaled

This figure gives a strong evidence that the dynamics outside islets is uniform. We can ask why the effect of the islets in this simple approximation is to decrease D_k. The reason is easy: the islets found around fixed points or points of period 2 or 4 are rather close to the values $x = 1/4, 3/4$ (see Section 4.1). But these are the values for which $(\Delta y)^2 = k^2 \sin(2\pi x)^2$ is maximal and close to k^2. As they are missing, the value of D_k decreases proportionally to the size of the islands.

A better approach takes into account the fact that, even if we discard the effect of the islets, values of x uniformly distributed for a given y, do not have the images uniformly distributed in x. This leads to correction factors which can be expressed in terms of Bessel functions. See, e.g., [34], Chapter 5, for background and details.

But, still, the approach is not satisfactory in the presence of islets. Preliminary computations show that the diffusive properties are destroyed due to the effect of some of the islets. Results in this direction will appear elsewhere, see [35], where the title is tentative.

6 Conclusions and outlook

In this work we have given a detailed and complete account of the dynamics of the well-known conservative Hénon map, with emphasis on the evolution of the measure of the set bounded orbits, on the confined chaotic orbits, on the splitting properties of the invariant manifolds of fixed and periodic points, and on the destruction of the invariant rotational curves surrounding most of the confined domain.

The paradigmatic character of this Hénon map, as a model for many other maps, and the fact that it appears as relevant model near tangencies of general area preserving maps [6], will allow to explain many of the general features observed in those maps.

A shorter study of the case of orientation-reversing Hénon map has also been presented.

It turns out that both maps are a key to understand the behaviour of the dominant islets in the Chirikov standard map for large values of the parameter. Both a theoretical approach and numerical comparisons with the results in the Hénon cases are presented.

Finally, preliminary considerations concerning some of the effects of these islands in the diffusive properties of the standard map are presented. Future work will be devoted to a complete clarification of the effect of the islands in the statistical properties of the Chirikov map, for values of the parameters for which some of the detected islands play a key role.

Acknowledgments

The authors have been supported by grants MTM2010-16425 (Spain) and 2009 SGR 67 (Catalonia). We thank J. Timoneda for the maintenance task of the computing facilities of the Dynamical Systems Group of the Universitat de Barcelona, that have been largely used in this work. We also thank Vered Rom-Kedar, Sergey Gonchenko, Marina Gonchenko and Vassili Gelfreich for fruitful discussions.

References

[1] Newhouse, S.E., Diffeomorphisms with infinitely many sinks. *Topology*, 1974, Vol. 13, pp. 9–18.

[2] Palis, J. and Takens, F., *Hyperbolicity and Sensitive Chaotic Dynamics at Homoclinic Bifurcations*, Cambridge Studies in advanced mathematics, Cambridge University Press, 1995.

[3] Gonchenko, S.V. and Shilnikov, L.P., On two-dimensional area-preserving mappings with homoclinic tangencies, *Russian Math. Dokl.*, 2001, Vol. 63, no. 3, pp. 395–399.

[4] Gonchenko, S.V. and Shilnikov, L.P., On two-dimensional area-preserving maps with homoclinic tangencies that have infinitely many generic elliptic periodic points, *Notes of the S. Petersburg branch of Steklov Math. Inst.*, 2003, Vol. 300, pp. 155–166.

[5] Gonchenko, S.V. and Gonchenko, V.S., On bifurcations of birth of closed invariant curves in the case of two-dimensional diffeomorphisms with homoclinic tangencies, *Trans. of Math.Steklov Inst.*, Moscow, 2004, Vol. 244.

[6] Gonchenko, M., *Homoclinic phenomena in conservative systems*, Ph.D. Thesis, Universitat Politècnica de Catalunya, 2013.

[7] Delshams, A., Gonchenko, S.V., Gonchenko, V.S., Lázaro, J.T. and Sten'kin, O., Abundance of attracting, repelling and elliptic periodic orbits in two-dimensional reversible maps, *Nonlinearity*, 2013, Vo. 26, pp. 1–33.

[8] Chirikov, B.V., A universal instability of many-dimensional oscillator systems, *Phys. Rep.*, 1979, Vol. 52, no. 5, pp. 264–379.

[9] Karney, C.F.F., Rechester, A. and White, B., Effect of noise on the standard mapping, *Physica D*, 1982, Vol. 4, no. 3, pp. 425–438.

[10] Hénon, M., Numerical study of quadratic area-preserving mappings, *Quart. Appl. Math.*, 1969, Vol. 27, pp. 291–312.

[11] Simó, C. and Vieiro, A., Resonant zones, inner and outer splittings in generic and low order resonances of Area Preserving Maps, *Nonlinearity*, 2009, Vol. 22, pp. 1191–1245.

[12] Sánchez, J., Net, M. and Simó, C., Computation of invariant tori by Newton-Krylov methods in large-scale dissipative systems, *Physica D*, 2010, Vol. 239, pp. 123–133.

[13] Simó, C. and Vieiro, A., A numerical exploration of weakly dissipative two-dimensional maps. In *Proceedings of ENOC-2005*, Eindhoven, Netherlands, 2005.

[14] Simó, C. Some properties of the global behaviour of conservative low dimensional systems. In *Foundations of Computational Mathematics: Hong Kong 2008*, Cucker, F. et al. editors, London Math. Soc. Lecture Notes Series, Vol. 363, pp. 163–189, Cambridge Univ. Press, 2009.

[15] Dumortier, F., Ibáñez, S., Kokubu, H. and Simó, C., About the unfolding of a Hopf-zero singularity, *Discrete Contin. Dyn. Syst. Ser. A*, 2013, Vol. 33, pp. 4435–4471.

[16] Fontich, E. and Simó, C., Invariant Manifolds for Near Identity Differentiable Maps and Splitting of Separatrices, *Ergod. Th. & Dynam. Sys.*, 1990, Vol. 10, pp. 319–346.

[17] Fontich, E. and Simó, C., The Splitting of Separatrices for Analytic Diffeomorphisms. *Ergod. Th. & Dynam. Sys.*, 1990, Vol. 10, pp. 295–318.

[18] Simó, C., Analytic and numeric computations of exponentially small phenomena. In Proceedings *EQUADIFF 99*, Berlin, Fiedler, B., Grögeri, K. and Sprekels, J., editors, World Scientific, Singapore, 2000, pp. 967–976.

[19] Gelfreich, V. and Simó, C., High-precision computations of divergent asymptotic series and homoclinic phenomena. *Discrete Contin. Dyn. Syst. Ser. B*, 2008, Vol. 10, pp. 511–536.

[20] Batut, C., Belabas, K., Bernardi, D., Cohen, H. and Olivier, M., *Users' guide to PARI/GP*, `http://pari.math.u-bordeaux.fr/`

[21] Arnold, V.I. and Avez, A., *Problèmes ergodiques de la mécanique classique*, Gauthier-Villars, Paris, 1967.

[22] Olvera, A. and Simó, C., An obstruction method for the destruction of invariant curves. *Physica D*, 1987, Vol. 26, pp. 181–192.

[23] Simó, C. and Treschev, D., Evolution of the "last" invariant curve in a family of area preserving maps. Preprint, 1998, see `http://www.maia.ub.es/dsg/1998/index.html`

[24] Simó, C., Invariant Curves of Perturbations of Non Twist Integrable Area Preserving Maps. *Regular and Chaotic Dynamics*, 1998, Vol. 3, pp. 180–195.

[25] Simó, C. and Vieiro, A., Dynamics in chaotic zones of area preserving maps: close to separatrix and global instability zones, *Physica D*, 2011, Vol. 240, no. 8, pp. 732–753.

[26] Chirikov, B.V. and Izraelev, F.M., Some numerical experiments with a nonlinear mapping: stochastic component. In *Colloques Internationaux du C.N.R.S. Transformations Ponctuelles et leurs Applications*, Toulouse, 1973.

[27] Simó, C., Analytical and numerical computation of invariant manifolds. In *Modern methods in celestial mechanics*, Benest, D. et Froeschlé, C., editeurs, Editions Frontières, 1990, pp. 285–330.

[28] Simó, C. and Treschev, D., Stability islands in the vicinity of separatrices of near-integrable symplectic maps, *Discrete Contin. Dyn. Syst. Ser. B*, 2008, Vol. 10, pp. 681–698.

[29] Simó, C. and Vieiro, A., Some remarks on the abundance of stable periodic orbits inside homoclinic lobes, *Physica D*, 2011, Vol. 240, pp. 1936–1953.

[30] Greene, J.M., A method for determining stochastic transition. *J. Math. Phys.*, 1979, Vol. 6, no. 20, pp. 1183–1201.

[31] Zaslavsky, G.M., Zakharov, M.Yu., Sagdeev, R.Z., Usikov, D.A. and Chernikov, A.A., Stochastic web and diffusion of particles in magnetic field, *Sov. Phys. JETP*, 1986, Vol. 64, pp. 294–303.

[32] Rom-Kedar, V. and Zaslavsky, G., Islands of accelerator modes and homoclinic tangles. *Chaos*, 1999, Vol. 9. no. 3, pp. 697–705.

[33] Chirikov, B.V., Chaotic dynamics in Hamiltonian systems with divided phase space. In *Proceed. Sitges Conference on Dynamical Systems and Chaos*, Garrido, L., editor, Lecture Notes in Physics, Vol. 179, Springer, 1983.

[34] Lichtenberg, A.J. and Lieberman, M.A., *Regular And Chaotic Dynamics*, Applied Mathematical Sciences, 2nd edition, Springer, New York, 1992.

[35] Miguel, N., Simó, C. and Vieiro, A., Destruction of the diffusive properties of the standard map, for large parameter values, due to the effect of some islands. Work in progress.